Journal of Inflammation Research

Dovepress
Taylor & Francis Group

Open Access Full Text Article

ORIGINAL RESEARCH

Pyroptosis-Related Genes as Prognostic Biomarkers and Immune Infiltration Features in Sepsis-Induced ARDS: A Single-Cell and Bulk RNA-Sequencing Analysis

Pan Zhang[1,*], Chun-Li Xu[2,*], Li Xu[1], Jing Jing Wu[3], Li Wang[4]

[1]Department of Emergency, Union Hospital, Tongji Medical College, Huazhong University of Science and Technology, Wuhan, 430022, People's Republic of China; [2]Department of Anesthesiology, Union Hospital, Tongji Medical College, Huazhong University of Science and Technology, Wuhan, 430022, People's Republic of China; [3]Department of Cardiology, Union Hospital, Tongji Medical College, Huazhong University of Science and Technology, Wuhan, 430022, People's Republic of China; [4]Department of Emergency Surgery, Union Hospital, Tongji Medical College, Huazhong University of Science and Technology, Wuhan, 430022, People's Republic of China

*These authors contributed equally to this work

Correspondence: Jing Jing Wu, Department of Cardiology, Union Hospital, Tongji Medical College, Huazhong University of Science and Technology, 1277 Jiefang Avenue, Wuhan, 430022, People's Republic of China, Email wujingjing@hust.edu.cn; Li Wang, Department of Emergency Surgery, Union Hospital, Tongji Medical College, Huazhong University of Science and Technology, 1277 Jiefang Avenue, Wuhan, 430022, People's Republic of China, Email wangli1229@hust.edu.cn

Background: Sepsis-induced acute respiratory distress syndrome (ARDS) is a common and costly syndrome with high mortality and poor prognosis without targeted therapies. Recently, pyroptosis has been demonstrated to be an inflammatory form of programmed cell death. However, the expression of pyroptosis-related genes (PRGs) in sepsis-induced ARDS and their correlation with prognosis remain unclear.

Methods: In this study, 760 sepsis samples from public datasets were analyzed. We first conducted a comprehensive analysis of single-cell RNA-sequencing data of sepsis from the Gene Expression Omnibus database and identified 8 cell types and 38 hub genes. Subsequently, we used univariate Cox hazard analysis to narrow down the candidate genes and developed a prognostic model using the disease cohorts, which stratified patients into high- and low-risk groups. Four genes associated with the prognosis of patients with sepsis admitted to the intensive care unit for ≥ 28 days were identified.

Results: High-risk patients have lower proportions of activated $CD8^+$ T, effector memory $CD8^+$ T, and memory B cells. The majority of the immune cells were positively correlated with each other. However, there was a negative association between neutrophils and other factors. Importantly, correlations between prognostic genes and the corresponding immune cells revealed that CCL5, CD3G, and IL7R were significantly associated with activated CD8+ T cells, and GIMAP4 was significantly negatively correlated with immune cells. Multivariate analysis identified the risk score as an independent prognostic factor.

Conclusion: PRGs play a significant role in sepsis immunity. The above four key genes (CCL5, CD3G, IL7R, and GIMAP4) are expected to serve as clinical diagnostic targets, providing a basis for clinical prognosis stratification in patients with sepsis-induced ARDS and guiding the formulation of individualized treatment strategies.

Keywords: sepsis, acute respiratory distress syndrome, pyroptosis-related genes, single-cell RNA-sequencing, prognosis

Introduction

Sepsis is a severe infectious disease characterized by life-threatening organ dysfunction and high mortality. Current sepsis morbidity and mortality estimates are concerning: 19.4 million new cases and 5.3 million fatalities occur each year.[1] Acute respiratory distress syndrome (ARDS) is a serious and fatal condition characterized by severe hypoxemic lung failure that necessitates mechanical ventilation.[2] Severe sepsis accounts for the highest proportion of

Received: 9 May 2025
Accepted: 8 September 2025
Published: 15 October 2025

all causative factors of ARDS, making it a significant risk element. An investigative study found that patients with sepsis-induced ARDS had a higher death rate and worse outcomes than non-sepsis-related ARDS.[3] Sepsis-induced ARDS, due to its high mortality rate and prognostic heterogeneity, urgently requires reliable prognostic biomarkers. The biomarkers that have been reported so far include inflammatory factors (such as IL-6, TNF-α), endothelial injury markers (such as soluble thrombomodulin, Ang-2), and coagulation function related indicators (such as D-dimer), but these markers have limitations such as insufficient specificity and difficulty in reflecting the dynamic progression of the disease. In addition, some studies have explored the role of pyroptosy-related genes (PRGS) in sepsis. For instance, the activation of NLRP3 inflammasome has been confirmed to be associated with lung injury in sepsis. However, most of these studies have focused on the mechanism verification of a single gene, lacking systematic analysis of the overall PRG network and immune associations. Therefore, investigating new prognostic biomarkers and incorporating them into a risk prediction model is crucial for improving the outcomes of patients with sepsis-induced ARDS.

Pyroptosis is a unique form of programmed cell death that initiates inflammatory reactions through gene-controlled cellular destruction, characterized by morphological changes such as cell swelling, membrane ballooning, lysis, and the release of pro-inflammatory cell contents.[4,5] This process is regulated by pyroptosis-related genes (PRGs), which contain a cascade of highly conserved regulators. Pyroptosis is not only a substantial contributor to the innate immune system's inflammatory response, causing tissue damage as a response to infection by recognizing various intracellular and extracellular stimulations but also plays a vital role in clearing pathogens and endogenous risk signaling.[6] Therefore, pyroptosis is a "double-edge sword". Pathological inflammatory responses occur when excessive caspase-1 is activated. The inhibition of pyroptosis in sepsis-induced acute lung injury is supported by studies demonstrating the effectiveness of inhibition of the C3A-C3AR complement axis and NLRP3.[7] Understanding how to balance the bidirectional effects may help explain how sepsis-induced ARDS or pyroptosis progresses. In sepsis-induced ARDS, a few PRGs perform broad and different biological functions.[8] These genes may serve as prospective therapeutic targets for the detection and prevention of sepsis-induced ARDS. However, a systemic understanding of PRGs and immune cell infiltration in sepsis-induced ARDS has not been fully elucidated, necessitating further exploration. This may facilitate the identification of potential biomarkers for the treatment of sepsis-induced ARDS.

Second-generation high-throughput RNA-sequencing (RNA-Seq) is a non-biased method for studying transcriptomic alterations in different disease states or under different treatment conditions.[9] To gain deeper insights into the genetic events associated with septicemia and shed light on its inflammatory etiology, we sought to identify differentially expressed genes (DEGs) in sepsis through bioinformatics analysis, leveraging Gene Expression Omnibus (GEO) data. Next, we performed functional enrichment and protein-protein interaction analyses to identify the most important signaling pathways of the DEGs. Clusters with high pyroptotic activity in sepsis were identified using the AUCell method. Additionally, intercellular connections within the microenvironment were investigated, leading to the identification of potentially crucial regulatory molecules from a single-cell dataset. In this study, we combined single-cell sequencing with bulk RNA-seq analysis to resolve the expression characteristics of PRG in sepsis-induced ARDS and the intercellular regulatory network (such as the interaction between CD8+T cells and NK cells through the MIF/MHC-I pathway) at the cell subtype level. A prognostic model based on four PRGS (IL7R, GIMAP4, CD3G, and CCL5) was constructed, which not only effectively predicted the 28-day survival rate of patients but also revealed the association between these genes and immune cell infiltration (such as activated CD8+T cells and memory B cells), providing potential targets for immunotherapy. The clinical translational value of PRG in sepsis-induced ARDS was expanded through verification on external datasets. The aim is to clarify the important molecular and cellular events in the lungs of patients with sepsis, understand the mechanism of immune infiltration, and provide new targets for potential treatments.

Materials and Methods

Acquisition and Pre-Processing of Bulk Transcriptome Data

This research relied on readily available data, with the primary source being GEO. Acquisition of the whole genome expression profiles for sepsis was facilitated by the R package "GEOquery" through the GEO database. GSE65682 comprises

760 samples from patients with sepsis and 42 normal controls obtained using the Affymetrix GPL13667 [HG-U219] human genome U219 Array platform. The current study followed the guidelines for accessing these databases.

Retrieval and Analysis of Single-Cell Sequencing Data

Drawing from the vast collection of single-cell sequencing data from the GEO database, we identified a dataset featuring four uncomplicated sepsis samples and three samples associated with sepsis-induced ARDS. To manage the raw data, we employed the Seurat R programming package, version 4.2.0, to import the data from the single cells of GSE151263.[10] Initially, cells and genes were filtered using the following criteria: first, cells with fewer than 300 genes were excluded; second, genes expressed in fewer than one cell type were eliminated; third, cells with gene expression levels between 300 and 2500 were retained; fourth, cells with fewer than 10% mitochondrial genes were retained; finally, cells with a unique molecular identifier count of < 10,000 were retained. The data were standardized using the normalized data function provided by Seurat R. Following standardization, we identified DEGs in individual cells, carefully considering the correlation between mean expression and dispersion. Principal component analysis using crucial principal components was then performed to facilitate graphical clustering. The harmonization technique was used to remove the batch influence of distinct samples. To cluster the data, we used the "FindClusters" function, which implements a clustering algorithm based on shared the nearest neighbor modularity optimization. This was applied to 19 principal components with a resolution of 0.8, which resulted in the identification of 12 distinct clusters. Executing the "Runtsne" function enabled us to carry out t-distributed random neighbor embedding (tSNE), visually representing cell clustering on the tSNE-1 and tSNE-2 axes. The "FindAllMarkers" function was used to identify the DEGs in each cell cluster. Seurat default parameters were used for the normalization of gene expression data. Cell type-specific markers were then used to identify cell groups and to calculate and evaluate the percentages of different cell types.

Pyroptosis-Related Gene Score

The pathways for each cell in the "AUCell" R package were scored using gene set enrichment analysis (GSEA). Based on the area under the curve (AUC) values of the 73 selected pyroptosis genes, gene expression rankings were constructed for each cell to evaluate the proportion of the gene set that was highly abundant in each cell. Higher AUC values were observed in the cells expressing a higher number of genes in the gene set. We obtained a list of genes related to pyroptosis from numerous literature sources.[11–15] The threshold for identifying active cells in the gene set was determined by using the "AUCell_exploreThresholds" function (R AUCell package; version 1.18.0). Subsequently, the AUC score of each cell was plotted on the tSNE for visualization of active clusters using the "ggplot2" (version 3.3.5) function of R.

Pseudo-Time Construction of a Single-Cell Trajectory

Monocle 2 uses reverse graph embedding to conduct a pseudo-time analysis.[16] Based on a user-defined gene list, a pseudo-time plot was generated to accommodate the differentiation processes that manifested a combination of branched and linear patterns. To analyze the population of active pyroptotic cells over pseudo-time, raw count data was normalized by calculating the size scale, which was used to infer the trajectories. Genes that were both highly distributed and highly expressed (with an empirical dispersion/dispersion fit of at least 1 and a mean expression of at least 0.1) were used to construct the pseudo-time trajectory.[17] For the parameters of the DDRTree algorithm, default values were selected. We used branched expression analysis modeling built into monocle 2 to further investigate these branching events. This assists in the identification of every gene exhibiting significant expression dependent on branching.[16] The expression patterns that were dependent on the branch were visualized as a heat map using monocle 2.

Cell Communication Analysis and Ligand–Receptor Expression

The CellChat objects were generated using the "CellChat" R package, taking into account the unique molecular identifier count matrix for both groups, namely, Control and Sepsis.[17] The "CellChatDB.human" ligand–receptor interaction database was preferred. Cell-to-cell communication analyses were performed using the default parameters. To compare the total number and strength of the interactions, the "mergeCellChat" function was used to merge the CellChat objects

from the two sets. The distinctions in the quantity or intensity of connections between unique cell types across groups were illustrated using the feature "netVisual_diffInteraction". Lastly, the functions "netVisual_bubbl" and "netVisual_aggregate" were used to display the distribution of signaling gene expression across the different groups.

Enrichment Analysis of the GO and KEGG Pathways

We conducted a comparative analysis of sepsis and sepsis-induced ARDS samples from the single-cell and bulk transcriptome datasets, and then intersected them with the differential genes of the pyroptosis-activated cell population set. The main DEGs related to pyroptosis were identified using intersecting groups. Gene ontology (GO)[18] enrichment analysis comprised analyses of biological processes (BP), molecular functions (MF), and cellular components (CC). The Kyoto Encyclopedia of Genes and Genomes (KEGG)[19] serves as a bioinformatics tool for identifying metabolic pathways significantly affected by alterations, as evidenced in the gene catalog. The "clusterProfiler" (version 4.2.2) R package was applied for GO and KEGG enrichment analyses ($p < 0.05$) of the significant DEGs.

Predictive System Development and Validation

Univariate Cox hazard analysis was used to assess the predictive significance of pyropathy-related DEGs and their association with the 28-day survival rate in the disease cohort. The genes associated with survival at $p < 0.05$ were identified for further analysis. A total of 177 disease samples remained after removing non-survival information and control samples. All samples with clinical information related to the disease were partitioned into two distinct sets: training (n = 118) and verification (n = 59) at a ratio of 7:3. This proportion selection is based on two considerations: First, to ensure that the sample size of the training set is large enough (about 70%) to fully capture the data distribution characteristics and stably construct the prognosis model, reducing the risk of model overfitting caused by insufficient sample size; Second, retaining 30% of the samples as the validation set can effectively assess the generalization ability of the model and balance the training accuracy of the model and the reliability of validation. Using the least absolute shrinkage and selection operator (LASSO) Cox regression model, facilitated by the R package "glmnet",[20] the list of potential genes was narrowed down and a predictive model generated. Determination of the penalty parameter (λ) relied on the minimum criteria. The risk scores were calculated using the following formula:

$$riskScore = \sum(genei) * Expression(genei)$$

$$(\mathrm{Coef}(\mathrm{gene_i}),\ \text{coefficient};\ \mathrm{Expression}\,(\mathrm{genei}):\ \text{gene expression level})$$

The median risk score was used to divide the training cohort into low- and high-risk subgroups. Kaplan–Meier analysis was used for prognostic intentions and the Log rank test used for significance. Evaluation of the efficiency of the prediction model was conducted using receiver operating characteristic (ROC) curves, with an AUC value of > 0.6 deemed adequate for assessing the performance of the diagnostic test. For the validation studies, the verification groups were further categorized into low- or high-risk subgroups. The results were then compared.

Construction and Verification of Nomogram

The clinical information collected from the GEO cohort included age, sex, and disease classification. In our regression model, we examined variables along with risk scores. Cox regression models were used for both the univariate and multivariate analyses. Furthermore, we designed a nomogram to estimate the 5-, 10-, and 15-day survival probabilities, and the risk score was used as a predictive factor. We created a nomogram by combining prognostic and clinical features using the R package "RMS". Both the risk score model and nomogram were evaluated using time-dependent ROC curves.

Gene Set Enrichment Analysis

Using computer-based analysis, GSEA[21] determines whether a predefined gene set exhibits consistent and significant dissimilarities between two biological conditions. A catalog of sorted genes, ranked by log2 fold change (FC), was subjected to GSEA analysis using the R package "clusterProfiler" (version 4.2.2). One thousand gene-set permutations

were performed for each analysis. The Molecular Signatures Database (MSigDB) c2.cp.kegg.v7.5.1. symbols[22] was uses as the basis for our study. The reference gene collection chosen for this study was the collections. Genes were identified as significantly enriched when the adjusted p was < 0.05.

Gene Set Variation Analysis

A gene set variation analysis (GSVA) was implemented to assess the biological function differences between the low- and high-risk groups, using the R package "GSVA" (version 1.42.0) and the "c2.cp.kegg.v7.5.1. symbols" dataset. R package "pheatmap" (version 1.0.12) was used to present the findings.

Analysis of Immune Infiltration

Single-sample GSEA (ssGSEA),[23] an extension of GSEA, computes distinct enrichment scores for individual sample/set pairs. The ssGSEA enrichment score indicates the collective upregulation or downregulation of genes within a specific gene set in a given sample. Unlike the traditional method of computing enrichment scores for probe and gene set groups, ssGSEA yields values for individual probe/gene set combinations. To quantify the relative enrichment score for each immunocyte, we used the 28 immune cell types (Activated CD8 T cell, Central memory CD8 T cell, Effector memory CD8 T, Activated CD4 T cell, Central memory CD4 T cell, Effector memory CD4 T cell, T follicular helper cell, Gamma delta T cell, Type 1 T helper cell, Type 17 T helper cell, Type 2 T helper cell, Regulatory T cell, Activated B cell, Immature B cell, Memory B cell, Natural killer cell, CD56bright natural killer cell, CD56dim natural killer cell, Myeloid derived suppressor cell, Natural killer T cell, Activated dendritic cell, Plasmacytoid dendritic cell, Immature dendritic cell, Macrophage, Eosinophil, Mast cell, Monocyte, Neutrophil) obtained from the Tumor and Immune System Interactions Database (TISIDB) and the gene expression profile of each disease sample.[24] The R package "ggplot2" (version 3.3.6) was used to plot the differential immune cell infiltration between the low- and high-risk groups.[25]

Prediction of Sepsis by Prognostic Model

83 sepsis samples and 28 healthy controls were included in this study as external validation by the sequencing platform of the GSE69528 dataset. The sequencing platform of the GSE69528 dataset was GPL10558 Illumina HumanHT-12 V4.0 expression beadchip.

Statistical Analysis

Correlations between the continuous variables in both groups were explored using the Wilcoxon signed-rank test. Proportions were compared using either the chi-square or Fisher's exact test. In R, survival curves based on Kaplan–Meier analysis were generated using the "ggsurvplot" function, facilitated by the "survminer" package. Statistical differences were examined using Log rank tests. Signature genes were established using LASSO-Cox regression, and predictive performance was assessed using ROC and time-ROC curves. The two-tailed p-value was set at a significance threshold of 0.05. The R software was used for all analyses (version 4.1.2).

Results

The step-by-step flow of the study is shown in the Figure 1.

Single-Cell Sequencing Analysis

To investigate the source of higher gene expression, we analyzed sepsis and sepsis ARDS cell populations using the single-cell sequencing dataset GSE151263. After performing an initial quality control assessment and removing doublets, 20369 cells were used to obtain single-cell transcriptome analyses. Figure 2A shows that the cells were uniformly distributed in both the sepsis and the control groups. The grouping of the cells into 12 clusters is shown in Figure 2B. Various cell types were labeled using cell-type-specific biomarkers based on the genetic characteristics of each cluster. As illustrated in Figure 2C, a total of eight cellular categories were identified: $CD4^+$T cells, $CD14^+$monocytes, $CD8^+$T cells, natural killer (NK) cells, B cells, monocyte-derived dendritic cells (Mo-DC), $CD16^+$monocytes, and megakaryocyte progenitor cells. Figure 2D provides a visual representation of the distribution of the different cell types in each sample. These data demonstrate the prevalence of $CD4^+$T cells, CD14

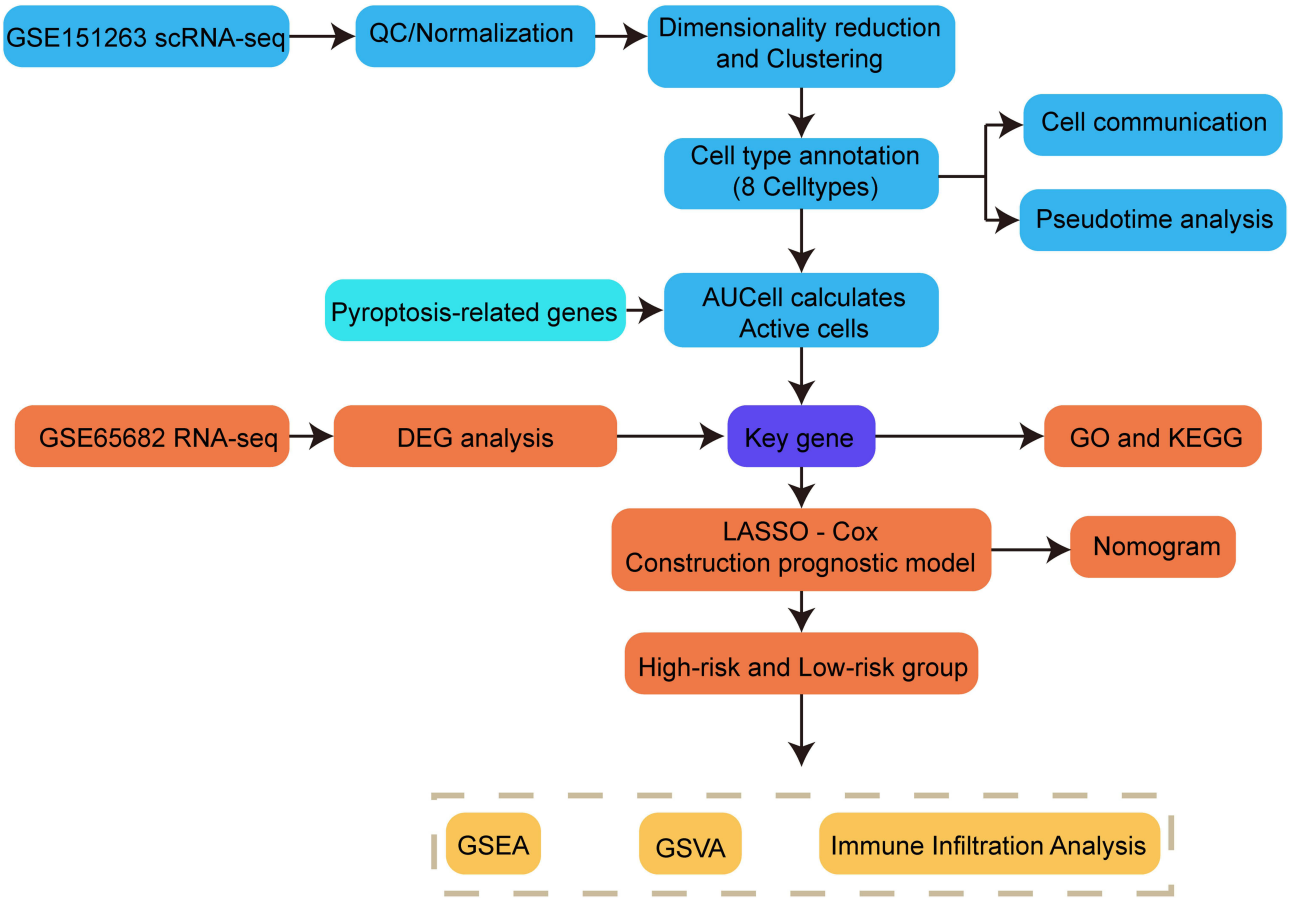

Figure 1 Procedural framework of the study.

+monocytes, $CD8^+$T cells, and NK cells in the analyzed samples. Specific genes for each cell type are visualized using dot plots (Figure 2E). IL7R, CTLA4, and CCR7 were detected in $CD4^+$T cells. NKG7, KLRD1, GZMB, and CD8A were expressed in NK cells. MS4A1, CD79B, CD79A, CD37, CD19, and BLNK were detected in B cells. GZMK, CD8B, and CD8A were detected in $CD8^+$T cells.

Pseudo-Time Analysis of Pyroptosis Active Cells

Investigation of PRG expression patterns involves the use of active cell subsets. We identified the inflection point of the density curve of AUC values, which corresponds to the boundary of the data distribution shifting from the "low-activity cluster" to the "high-activity cluster". Combining biological significance and research objectives, 0.18 corresponds to the inflection point in the distribution and was therefore selected as the threshold. The 197 cells that actively underwent pyroptosis were detected using the preferred threshold (Figure 3A). Cell populations exhibiting AUC values > 0.18 demonstrated high pyroptosis activity, whereas those with AUC values < 0.18 exhibited low activity (Figure 3B and C).

Using definitively highly pyroptosis-active cells, we constructed a transcriptional trajectory to identify the crucial gene expression programs governing sepsis progression. Transcriptional states along the trajectory revealed different courses. In the trajectory, the initial segment contained NK and $CD8^+$T cells, while $CD14^+$ monocytes occupied the endpoint, transitioning from $CD4^+$T cells (Figure 3D–F). The main cell types in each state were NK cells, $CD4^+$T cells, and $CD14^+$ monocytes (Figure 3G). To ascertain the molecular underpinnings of this transformation, we investigated the genes that dictate the fate of septic cells. Genes enriched in pathways such as secretory granulole lumen, cycloplastic vessel lumen, and vessel lumen were highly expressed in cell branch 1, while genes highly expressed in the pre-branch were mainly enriched in cell number homeostasis, negatively regulating the innate immune response, and myeloid cell

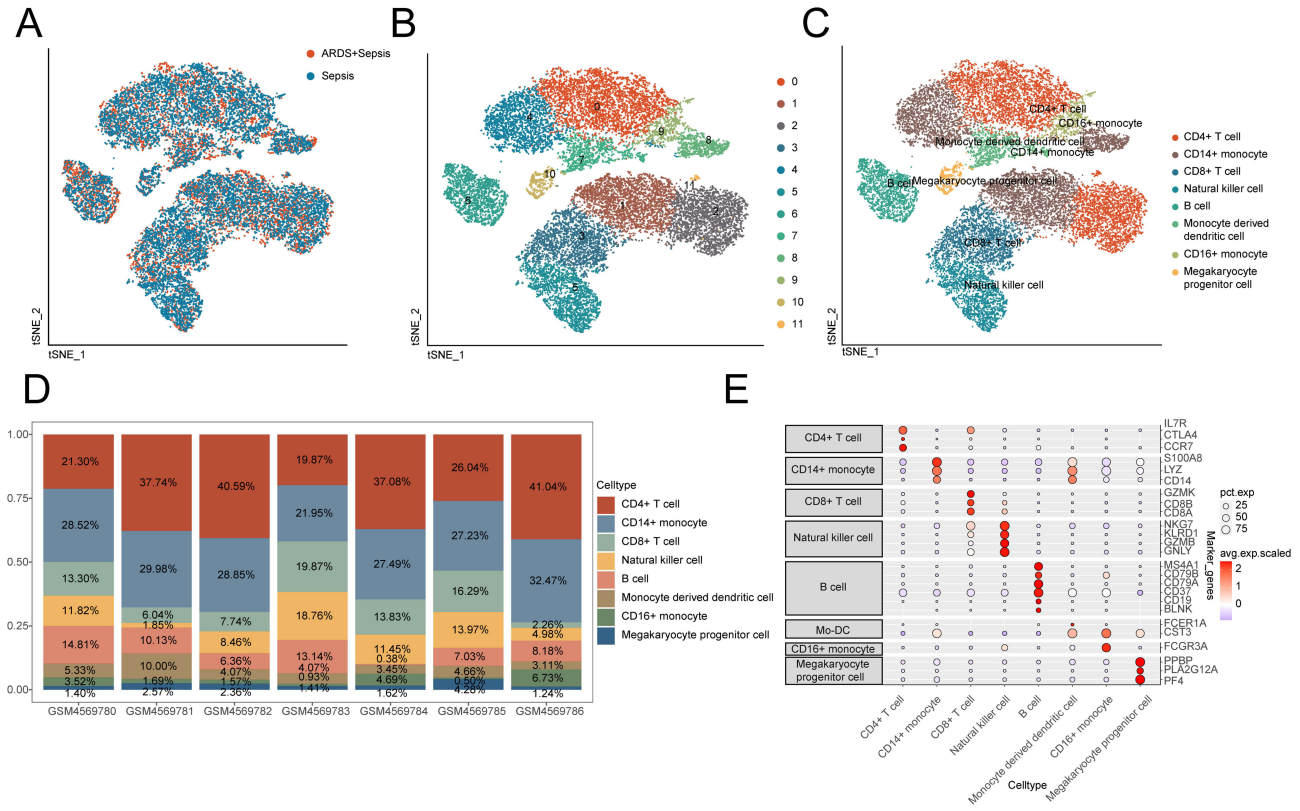

Figure 2 Identification of cellular subsets and marker gene expression. (**A**) t-distributed random neighbor embedding (tSNE) map illustrates the sepsis and acute respiratory distress syndrome (ARDS) sample distribution. (**B**) tSNE map illustrates the cell subgroup distribution in sepsis. (**C**) tSNE map illustrates the annotation findings of distinct cell subgroups in sepsis. (**D**) Cumulative histogram presenting cell type distribution in samples taken from patients with sepsis and ARDS. (**E**) Marker gene expression profiles for every cell type.

homeostasis. Genes enriched in the defense responses to viruses, defense responses to symbionts, and ficolin-1-rich granules were also highly expressed (Figure 3H).

Cellular Communication Patterns in Sepsis Microenvironment

To further investigate the cellular interaction network in the sepsis microenvironment, our study used the "CellChat" R package to reveal alterations in cell crosstalk between ARDS tissue and controls, using sepsis as control. There was a decrease in the quantity and intensity of cellular interactions in ARDS tissues compared to the control (Figure 4A) and a decrease in the quantity and intensity of most interactions between immune cells (Figure 4B). These results indicated that the microenvironment is a complex milieu. We also compared the signal patterns between tissues from control populations and patients with sepsis-ARDS. The incoming signal patterns of sepsis and sepsis-ARDS are shown in Figure 4C. For example, the strength of the MHC-I signal acting on NK cells is enhanced in ARDS.

In addition, we analyzed receptor ligands that may regulate CD8+ T cell communication with other cells, and the results suggested that the MIF and MHC-I signaling pathways are important in sepsis. The MIF and MHC-I ligands derived from CD8+ T cells bound to the corresponding receptors on NK cells, and this interaction was increased in ARDS (Figure 4D and E).

We further investigated the expression of the MIF and MHC-I pathway genes in different cells between septic ARDS tissue and sepsis (Figure 4F–I) because CD8+ T cells mainly interact with NK cells through the MIF and MHC-I pathways. The most elevated expression distribution of MIF signaling genes in septic ARDS tissues involved CD16+ monocytes, whereas HLA is involved in megakaryocyte progenitor cells.

https://doi.org/10.2147/JIR.S539379

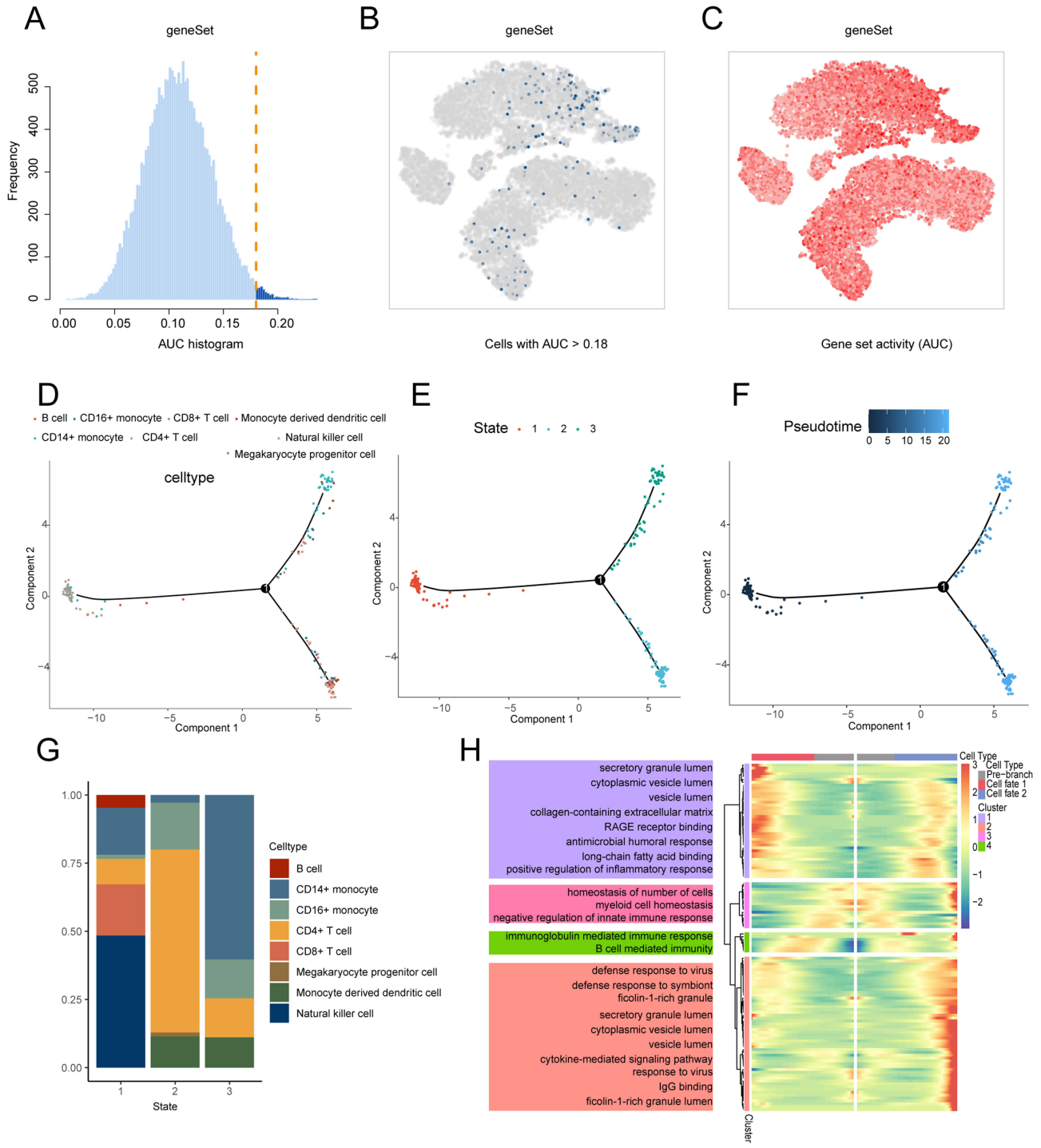

Figure 3 Transcriptional trajectory analyses reveal pyroptosis active cell transcriptional pattern. (**A**) Pyroptosis-related gene area under the curve (AUC) scores was calculated using a threshold of 0.18. (**B**) Cells with AUC values greater than the threshold are spatially represented on the t-distributed random neighbor embedding (tSNE) colorogram. (**C**) The tSNE colorogram displays the level of cellular activity. A brighter color represents higher activity. (**D**) Pseudo-temporal trajectory demonstrating the distribution of cells in sepsis categorized by cell type. (**E**) Monocle 2 classifies the pseudo-time trajectory into three distinct states. (**F**) Pseudo-time color gradient transitions from dark blue to light blue. (**G**) Cumulative histogram provides a visual overview cell type distribution across different states. (**H**) Heatmap of differentially expressed genes of different cell fates. The top gene ontology pathways from each cluster are shown next to the heat map.

Enrichment Analysis of DEGs Associated with Pyroptosis in Sepsis

In the single-cell RNA dataset, a comparison between sepsis and sepsis-related ARDS samples identified 290 genes (DEG1) with statistically significant differences (adjusted $p < 0.05$, $|Log2FC| > 0.25$). In the bulk transcriptome dataset, a comparison between the sepsis and normal group identified 1404 genes (DEG2) with statistically significant differences (adjusted $p < 0.05$, $|Log2FC| > 1$). The heatmaps in Figure 5A illustrate the top five upregulated (S100A8, S100A12, MCEMP1, ANXA3, and ARG1) and top five downregulated genes (EPHX2, NMT2, P2RY10 C, CD160, and CCR6) in the sepsis samples. There were 605 genes (DEG3) between the pyroptosis-active and-inactive cells, with statistically significant differences (adjusted $p < 0.05$, $|Log2FC| > 0.25$). Intersection of the three sets of DEGs yielded 38 hub genes (Figure 5B).

For an in-depth understanding of the biological functions attributed to the hub genes, we carried out enrichment analysis of GO terms and displayed them using chord, circle, and lollipop plots. The GO results showed that these genes participate in various BPs, including "dendritic cell antigen processing ID description and presentation", "T cell differentiation", and "lymphocyte differentiation"; CCs such as "clathrin − coated endocytic vessel membrane", "clathrin − coated endocytic vessel", "clathrin − coated vessel membrane"; MFs such as "peptidase regulator activity", "protein binding", "cysteine type endopeptidase inhibitor activity" (Figure 5C–E). This suggests that these genes act synergistically in the immune microenvironment and contribute to the pathogenesis of sepsis-induced ARDS. Nevertheless, further research is essential to discern specific distinctions in the infiltration of immune cells and prognostic genes across various groups.

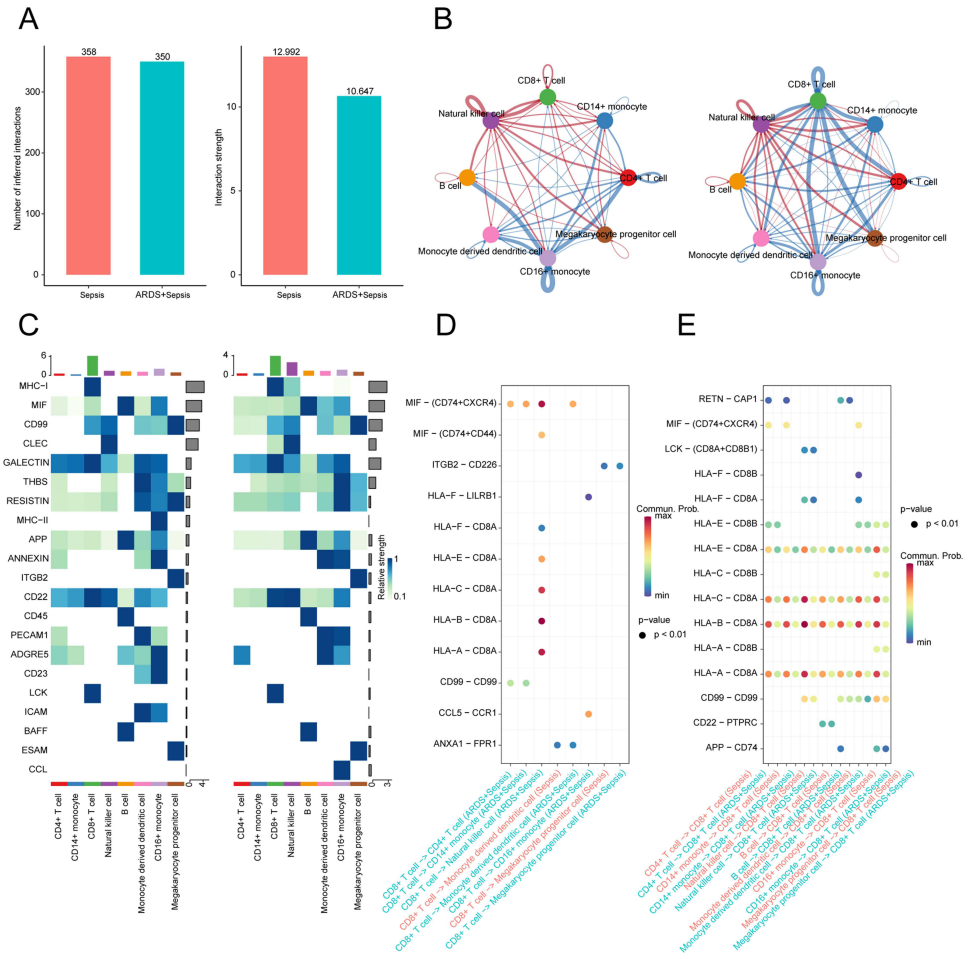

Figure 4 Continued.

https://doi.org/10.2147/JIR.S539379

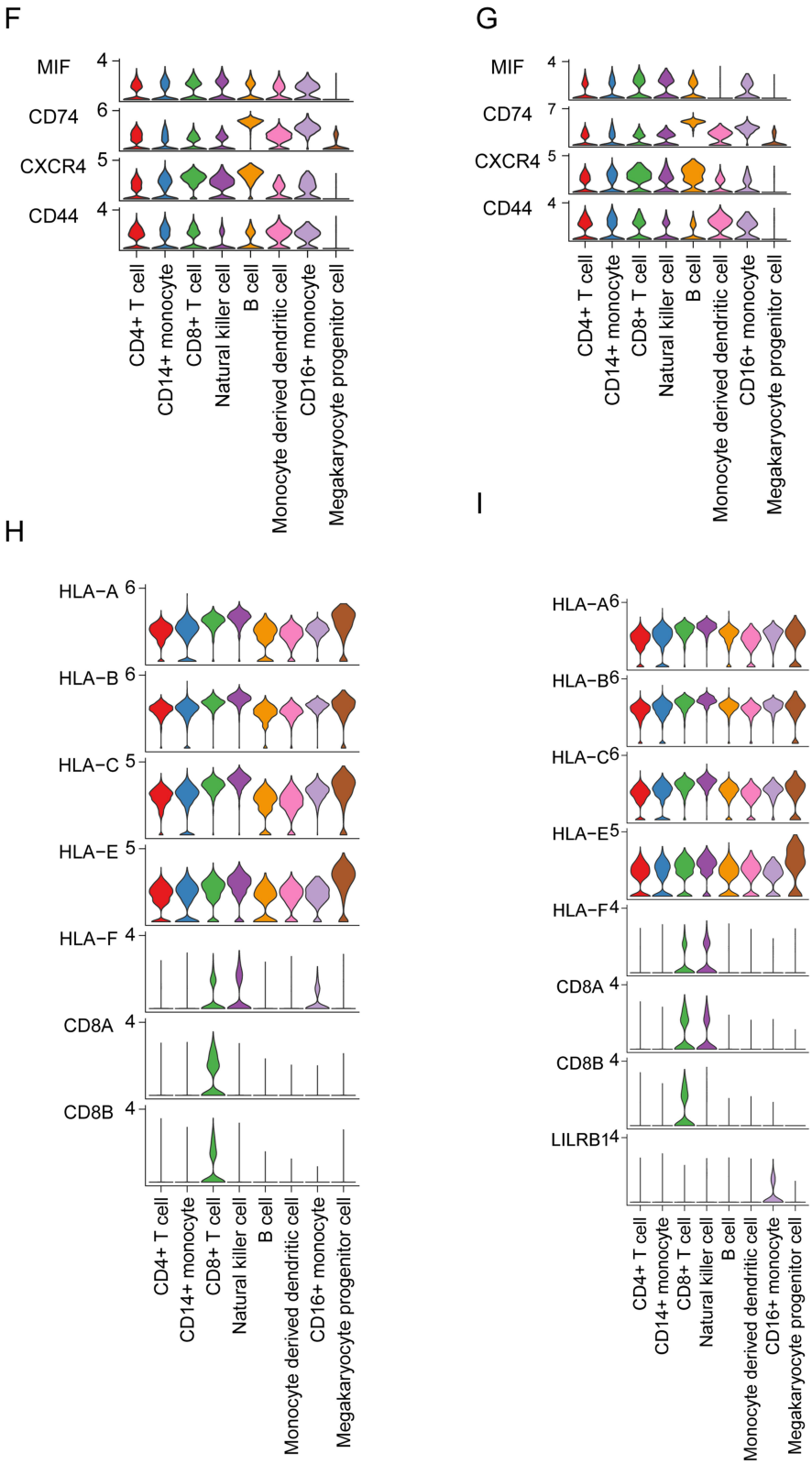

Figure 4 Intercellular communication analysis of septic ARDS and sepsis. (**A**) The bar plot shows the amount and intensity of sepsis-related ARDS and sepsis interaction. (**B**) The network diagram shows the amount and intensity of sepsis-related ARDS and sepsis interaction, differential number of interactions (left) and differential interactions strength(right). (**C**) The heatmap depicts the signal pathways received by cells in sepsis-related ARDS and sepsis tissues, incoming signaling patterns-Sepsis (left) and ARDS +Sepsis (right). (**D**) Increased ligand–receptor pairings involving CD8+ T cells and other cellular entities in septic ARDS. (**E**) Reduced ligand–receptor pairings involving CD8+ T cells and other cellular entities in septic ARDS. (**F**) Expression distribution of MIF signaling genes in septic ARDS tissues. (**G**) Distribution of gene expression of MIF signaling in septic tissues. (**H**) MHC-I-signaling gene expression and distribution in septic ARDS. (**I**) Distribution of gene expression of MHC-I signaling in septic tissues.

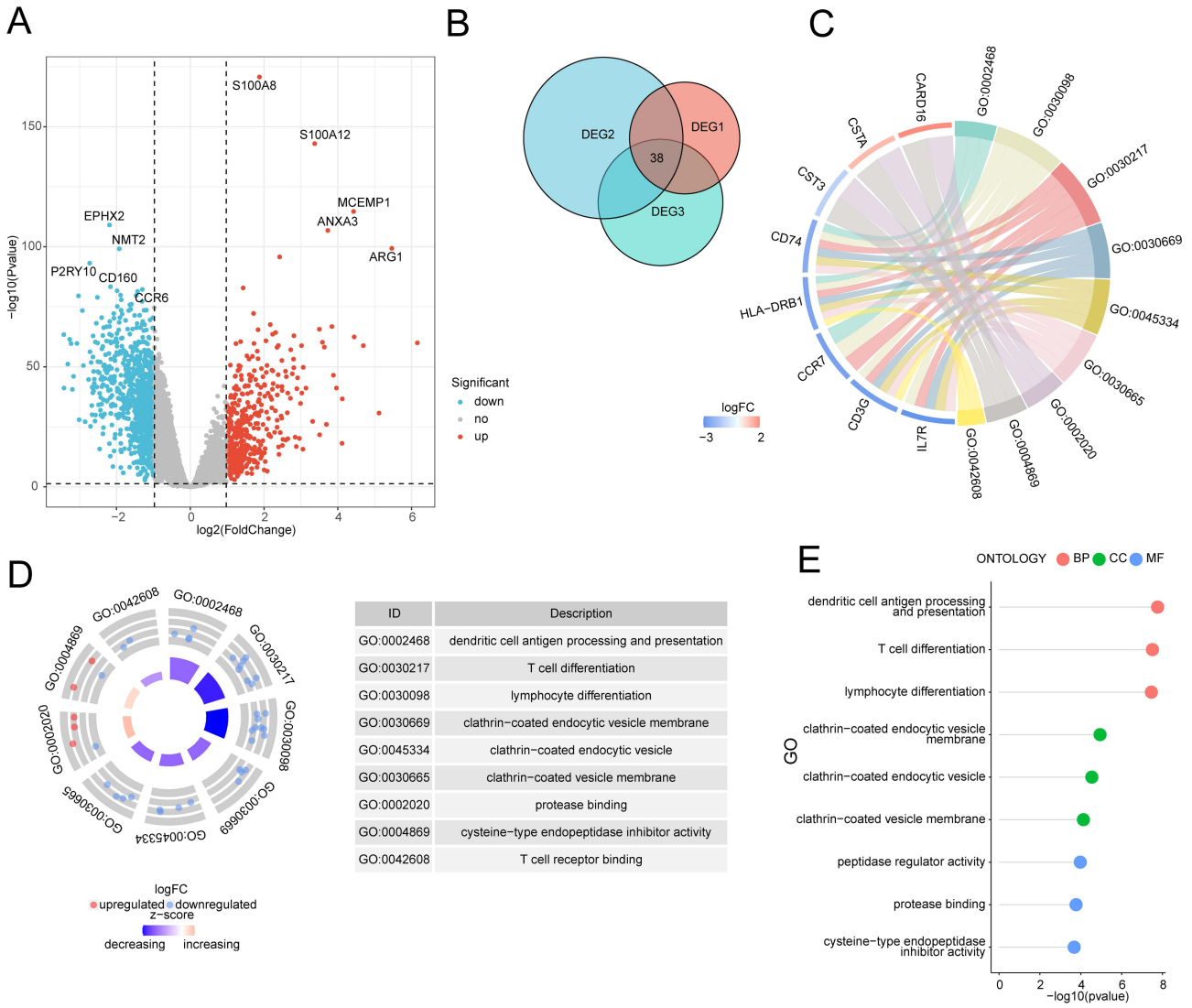

ID	Description
GO:0002468	dendritic cell antigen processing and presentation
GO:0030217	T cell differentiation
GO:0030098	lymphocyte differentiation
GO:0030669	clathrin−coated endocytic vesicle membrane
GO:0045334	clathrin−coated endocytic vesicle
GO:0030665	clathrin−coated vesicle membrane
GO:0002020	protease binding
GO:0004869	cysteine−type endopeptidase inhibitor activity
GO:0042608	T cell receptor binding

Figure 5 Enrichment analysis of differentially expressed genes related to pyroptosis activity. (**A**) Volcanic map depicting the genes with significant expression differences in sepsis compared to the control group. (**B**) Venn diagram depicting the overlap of three distinct sets of differentially expressed genes. (**C**) Chord plot displaying the enrichment in gene ontology (GO) terms for the hub genes. (**D**) Circle diagram displaying the enrichment in GO terms for the hub genes. (**E**) Lollipop plot displaying the enrichment in GO terms for the hub genes.

Prognostic Risk Model Construction and Verification

Univariate cox analysis was conducted on the 38 hub genes ($p < 0.05$) to identify the signature genes. Ultimately, ten genes associated with sepsis prognosis were identified. In this study, 70% of the septic samples were randomly chosen for the training set (n = 118), leaving the remaining 30% to form the validation set (n = 59). The training set was subjected to LASSO regression analysis to remove unnecessary genes. We identified four genes linked to the 28-day prognosis of intensive care unit-admitted patients with sepsis (Figure 6A and B). Classification of samples into high- and low-risk groups, as determined by the median risk value, was used to evaluate the stability of the models incorporating the four gene signatures. The training (Figure 6C) and validation cohorts (Figure 6D) underwent Kaplan–Meier survival curve analysis to elucidate patient outcomes within the distinct groups. In all cohorts, the findings indicated a notably poorer prognosis among the high-risk group than among their lower-risk counterparts. To assess the effectiveness of the model in predicting patient prognosis, an ROC curve was constructed (Figure 6E and F). The training cohort exhibited ROC

https://doi.org/10.2147/JIR.S539379

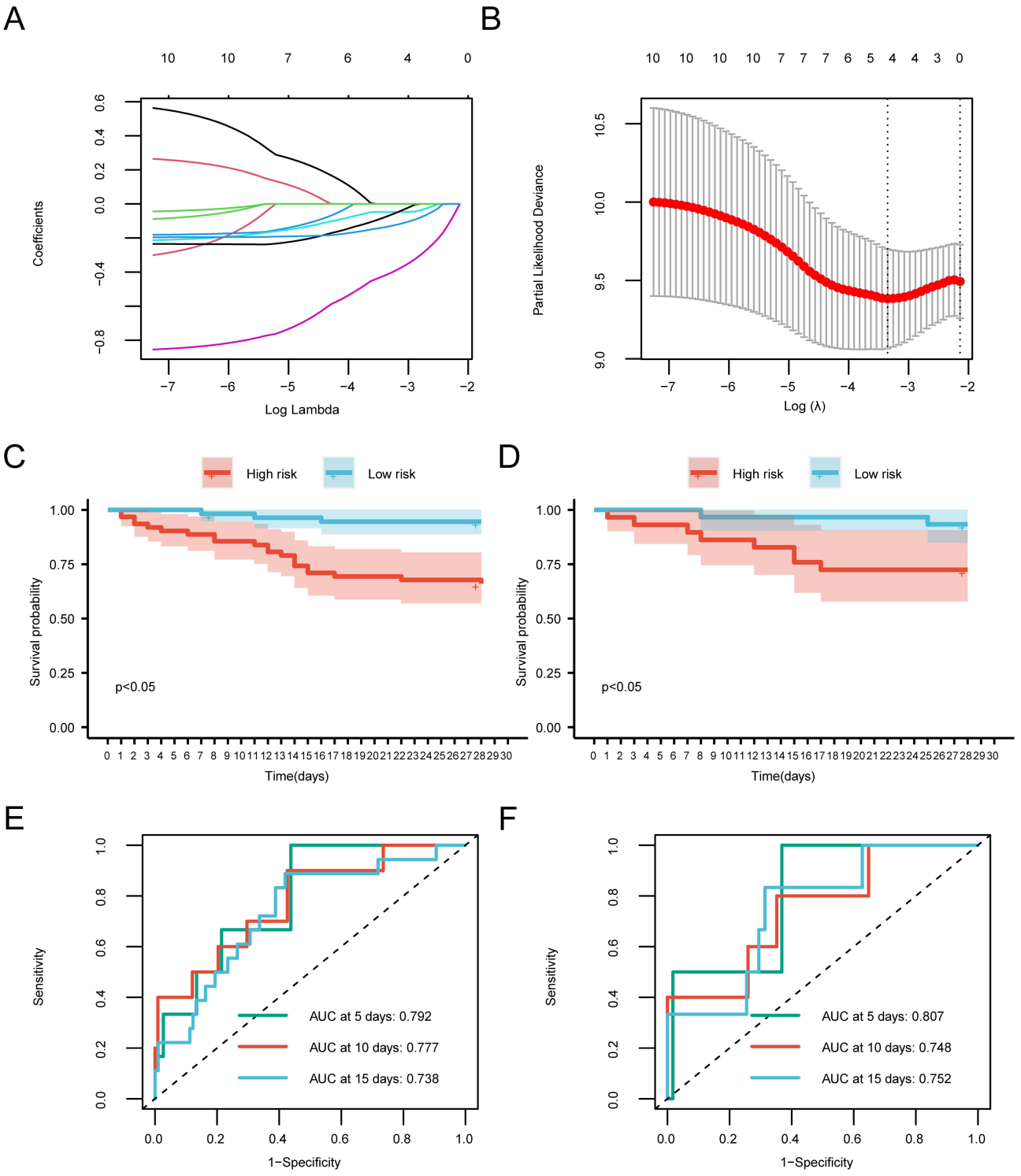

Figure 6 Cox and least absolute shrinkage and selection operator (LASSO) regression analysis in the sepsis dataset. (**A**) Changing trajectory of the LASSO regression of the independent variable, with the x-axis denoting the logarithm of the independent variable lambda and y-axis denoting the coefficient value. (**B**) LASSO regression confidence interval for each lambda. (**C**) Survival curve delineating patients within the training cohort from those of the higher and lower risk cohorts. (**D**) Survival curves delineating high-risk and low-risk groups of patients within the validation cohort. The high-risk group is highlighted in red, while the low-risk group is differentiated in blue in the graphical representation. (**E**) Receiver operating characteristic (ROC) curves for 5-, 10-, and 15-day time-dependent analyses for the models in the training cohorts. (**F**) ROC curves for 5-, 10-, and 15-day time-dependent analyses for the models in the validation cohorts.

values of 0.792, 0.777, and 0.738 for 5-, 10-, and 15-day survival, respectively, as shown in Figure 6E. The validation cohort exhibited ROC values of 0.807, 0.748, and 0.752 for 5-, 10-, and 15-day survival, respectively (Figure 6F).

Expression of Prognostic Genes in Different Cell Clusters

Next, we displayed the prognostic gene expression in various cell types using a heatmap (Figure 7A). The findings showed that the prognostic genes were expressed at low levels in most cell types. Specifically, High IL7R expression was observed in CD4+ T cells, in contrast to the low expression of most prognostic genes in NK cells, except for CCL5. CD8+ T, NK, and megakaryocyte progenitor cells exhibited high expression levels of CCL5.

Employing GSEA, we aimed to further elucidate the potential mechanisms underlying the DEGs in sepsis. The most significantly enriched pathways were identified and prioritized from the MSigDB collection based on normalized enrichment scores. GSEA identified ESTARCH AND SUCROSE METABOLISM (Figure 7B), CARDIAC MUSCLE CONTRACTION (Figure 7C), JAK STAT SIGNALING PATHWAY (Figure 7D), TYPE I DIABETES MELLITUS (Figure 7E), GRAFT VERSUS HOST DISEASE (Figure 7F), and ANTIGEN PROCESSING AND PRESENTATION ($p < 0.05$, Figure 7G) as significantly enriched in sepsis. In addition, we used the MSigDB collection for GSVA analysis and selected 11 pathways with the most significant differences (with the smallest p value) in the high- and low-risk groups to plot the pathway activity heatmap (Figure 7H). The low-risk groups showed enrichment of immune-related pathways, including the T CELL RECEPTOR SIGNALING PATHWAY, NOTCH SIGNALING PATHWAY, and some immune-related diseases.

Immune Infiltration

The 28 immune cell types and their corresponding marker gene sets used in this study were all obtained from TISIDB. As immunity is crucial in sepsis, we correlated prognostic genes with immune cell infiltration. Firstly, ssGSEA was used to measure the infiltration levels of 28 immune cell types in both high- and low-risk populations. In addition to activated B and CD4 T cells, substantial differences were noted in various immune cell types, including activated CD8 T and dendritic cells, between the high- and low-risk groups ($p < 0.05$; Figure 8A). High-risk patients are characterized by an increased proportion of activated dendritic, CD56bright NK, CD56dim NK, central memory CD4 T, central memory CD8 T, effector memory CD4 T, gamma delta T, immature dendritic, macrophage, mast, monocyte, NK, plasmacytoid dendritic, regulatory T, T follicular helper, type 1 T helper, and type 17 T helper cells, coupled with a decreased proportion of activated CD8 T, effector memory CD8 T, and memory B cells. Subsequently, we investigated further using a correlation analysis that specifically focused on immune cells. Most immune cell populations were correlated with each other. Figure 8B shows the negative correlation between neutrophils and other immune cells.

Furthermore, we identified significant correlations between the prognostic genes and the corresponding immune cells (Figure 8C–K). It should be noted that, genes CCL5 ($R = 0.4891$), CD3G ($R = 0.7072$), and IL7R ($R = 0.5977$) were significantly associated with activated CD8 T cells (Figure 8C, D, and F); GIMAP4 was significantly negatively correlated with immune cells including activated dendritic (Figure 8G), CD56bright NK (Figure 8H), immature dendritic (Figure 8I), macrophage (Figure 8J), and plasmacytoid dendritic cells (Figure 8K) ($p < 0.001$).

Construction and Verification of Nomogram

To investigate the potential autonomous prognostic role of the risk score in sepsis, we performed univariate cox regression analysis on key patient characteristics such as age, risk, and sex. It was also an independent prognostic risk factor (Figure 9A). A nomogram was constructed using multivariate cox regression analysis, which revealed a substantial predictive capability of the risk score for clinical outcomes (Figure 9B). The calibration curves of the 5-, 10-, and 15-day survival predictions were consistent with the actual results (Figure 9C), indicating that the nomogram had good prediction accuracy. We assessed the nomogram's predictive effectiveness for patient prognosis using ROC curve analysis. Figure 9D shows AUC values of 0.815, 0.790, and 0.752 for the 5-, 10-, and 15-day survival rates, respectively. These findings confirmed that the risk score independently predicts the development of sepsis.

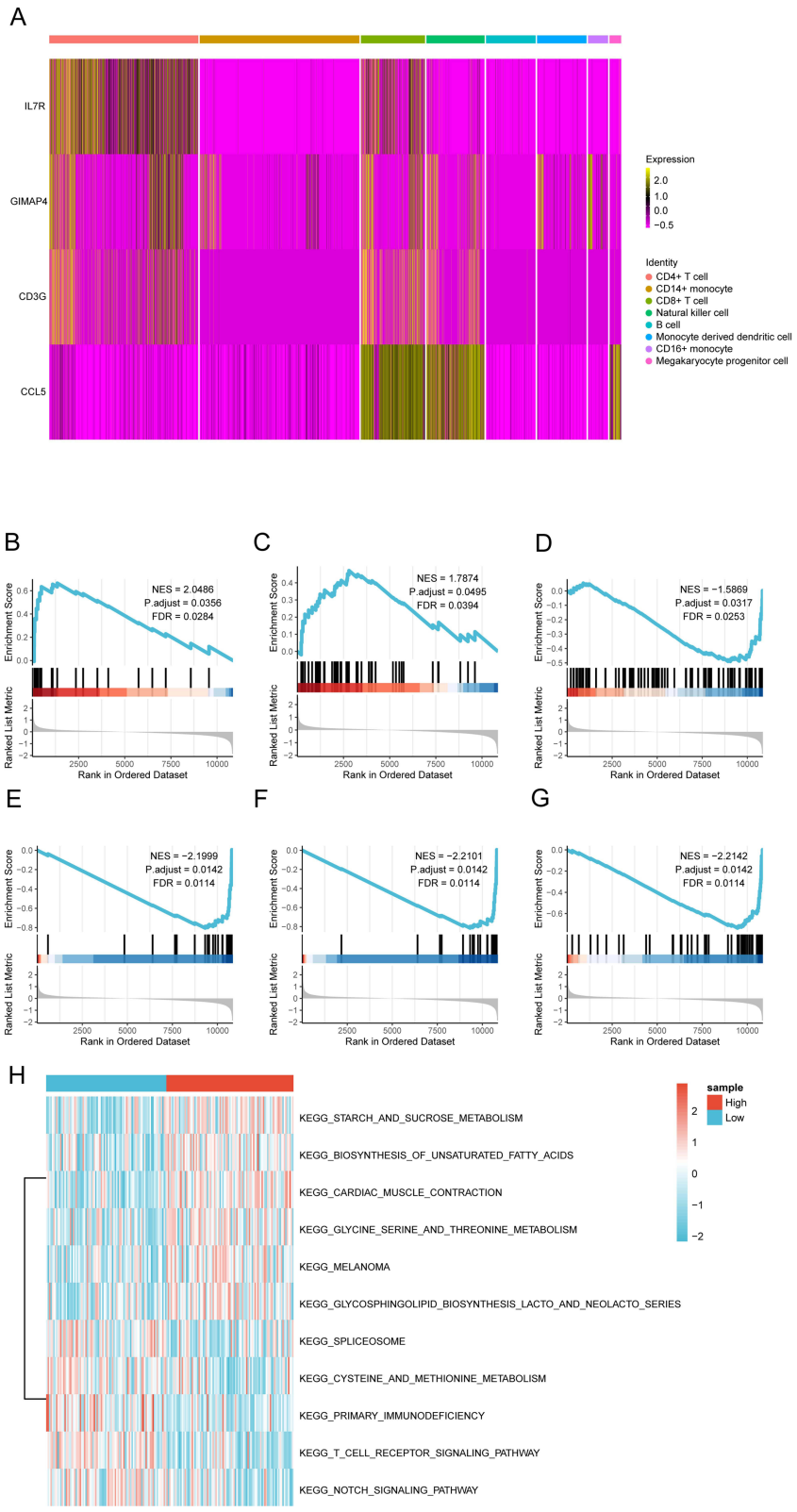

Figure 7 Gene set enrichment analysis and gene set variation analysis of significantly enriched pathways. (**A**) Heatmap displaying a visual representation of prognostic gene expression within various cell clusters, (**B**) STARCH AND SUCROSE METABOLISM, (**C**) CARDIAC MUSCLE CONTRACTION, (**D**) JAK STAT SIGNALING PATHWAY, (**E**) TYPE I DIABETES MELLITUS, (**F**) GRAFT VERSUS HOST DISEASE, and (**G**) ANTIGEN PROCESSING AND PRESENTATION. (**H**) Heatmaps of pathways enriched between high- and low-risk groups analyzed using gene set variation analysis enrichment.

Predictive Validation of Sepsis by Prognostic Model

In order to explore the diagnostic performance of the prognostic model for sepsis, ROC curve (Figure 10A–E) was performed based on the expression of riskScore and prognostic genes in the sepsis data set. The results showed that both riskScore and prognostic genes had good predictive accuracy as diagnostic basis (AUC > 0.9). Furthermore, the diagnostic efficiency of riskScore and each gene was further verified in independent data set GSE69528 (Figure 10F–I), in which the AUC values of riskScore, IL7R, CD3G and CCL5 were all greater than 0.7. It also showed that both riskScore and prognostic genes had good diagnostic value.

Discussion

Sepsis, a critical and life-threatening illness, is a major instigator of ARDS, stemming from an uncontrolled host reaction to infection.[26] Owing to the heterogeneity of sepsis and lack of targeted treatment, patients with sepsis often quickly progress to ARDS, resulting in a poor prognosis with high mortality rates. Immune cell infiltration is important for sepsis

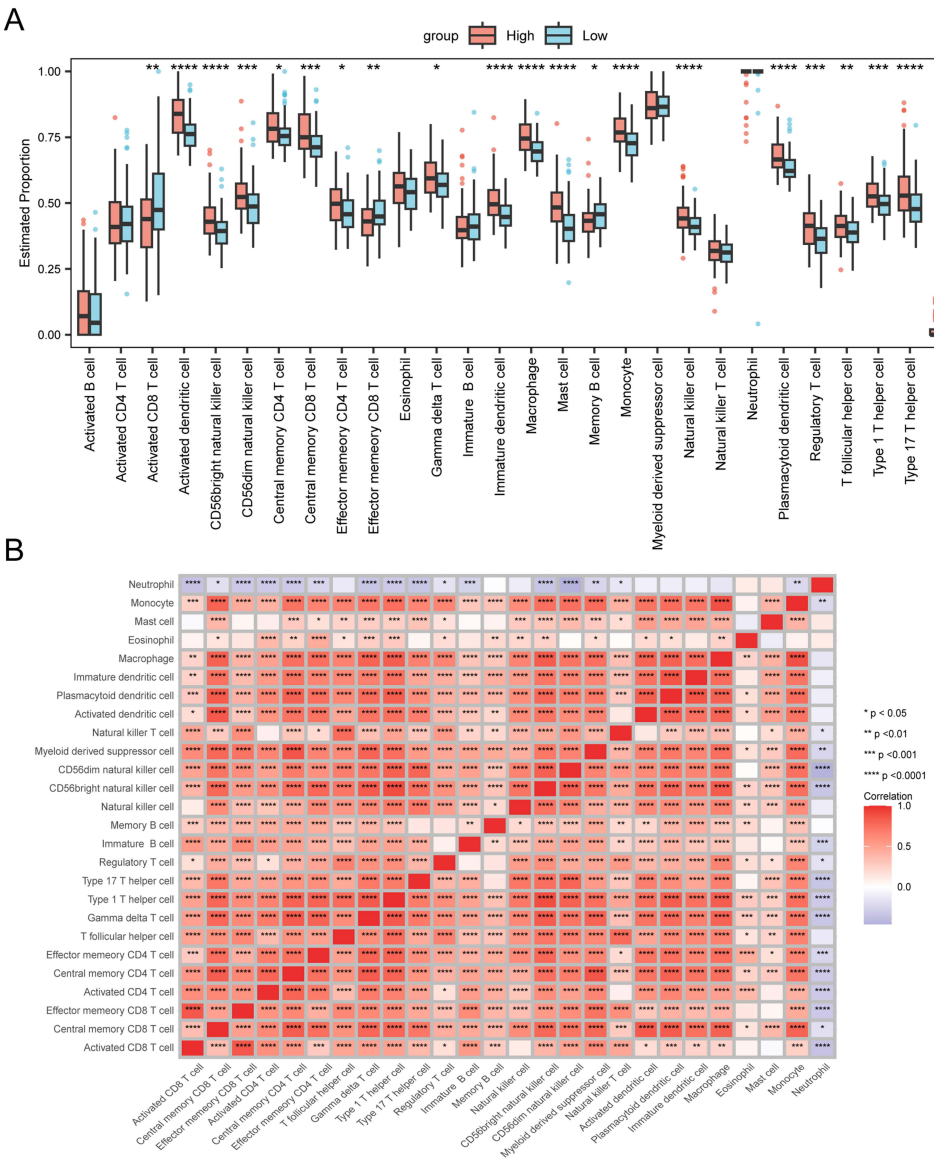

Figure 8 Continued.

https://doi.org/10.2147/JIR.S539379

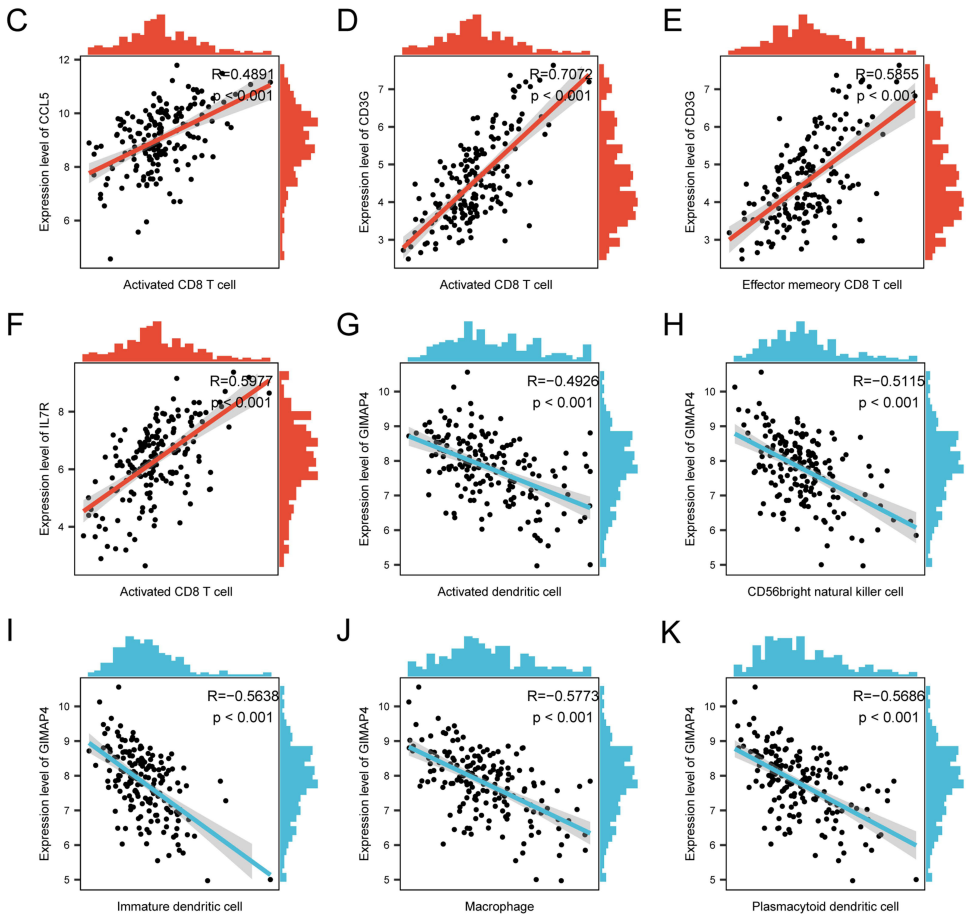

Figure 8 Immune infiltration levels between the high- and low-risk groups and immune cell-gene correlation. (**A**) The estimated proportions of 28 types of immune cells between the high- and low-risk groups. (**B**) Immune cell correlations. Correlation between CCL5 (**C**), CD3G (**D**) and activated CD8 T cells, and scatter plot of correlation between CD3G (**E**) and effector memory CD8 T cells. Correlation between IL7R (**F**) and activated CD8 T cells. Correlation between GIMAP4 and activated dendritic (**G**), CD56bright natural killer (**H**), immature dendritic (**I**), macrophage (**J**), and plasmacytoid dendritic cells (**K**). ****p < 0.0001, ***p < 0.001, **p < 0.01, *p < 0.05.

development, including macrophages, the alternative complement pathway, and myeloid cells.[27] Identifying distinct prognostic markers and scrutinizing immune cell infiltration patterns in sepsis are pivotal for improving the prognosis of individuals affected by this condition. With the rapid growth in science and technology, bioinformatics has become a potent approach for screening molecular markers. Investigating prognostic markers of sepsis and analyzing the involvement of immune cell infiltration were the core objectives of this study.

Using single-cell sequencing in the current investigation, we examined seven samples and identified eight distinct cell types, including $CD4^+$ T, NK, B, and$CD8^+$ T cells, $CD14^+$ monocytes, monocyte derived dendritic cells, $CD16^+$ monocytes, and megakaryocyte progenitor cells. Additionally, we identified 73 pyroptosis genes and assessed their biological activities using the PRG scoring algorithm. The most frequently observed cells with high PRG scores were NK, $CD8^+$ T, and CD4+ T cells, and $CD14^+$ monocytes. Studies have demonstrated that the promotion of inflammation during sepsis is significantly influenced by NK cells, irrespective of their functions in immunosurveillance and viral clearance.[28] In sepsis, the quantities and functional reactions of CD8+ T cells are compromised, resulting in an increased susceptibility to secondary infections and unfavorable consequences.[29] To investigate how these activities are associated with septic progression, we noted that NK and CD8+ T cells predominantly initiate the onset of the trajectory (cell fate 1), which reveals the change in state during sepsis progression. Further investigations focused on the genes influencing the fate of Cell 1, characterized by enrichment in immune-related pathways, and Cell 2, characterized by enrichment in pathways associated with cell communication. We found that numerous vesicular signaling pathways are involved in the pathogenesis of innate immunity, including various vesicles that coordinate the actions of immune cells during infection and inflammation. Extracellular vesicles (EV) refer to

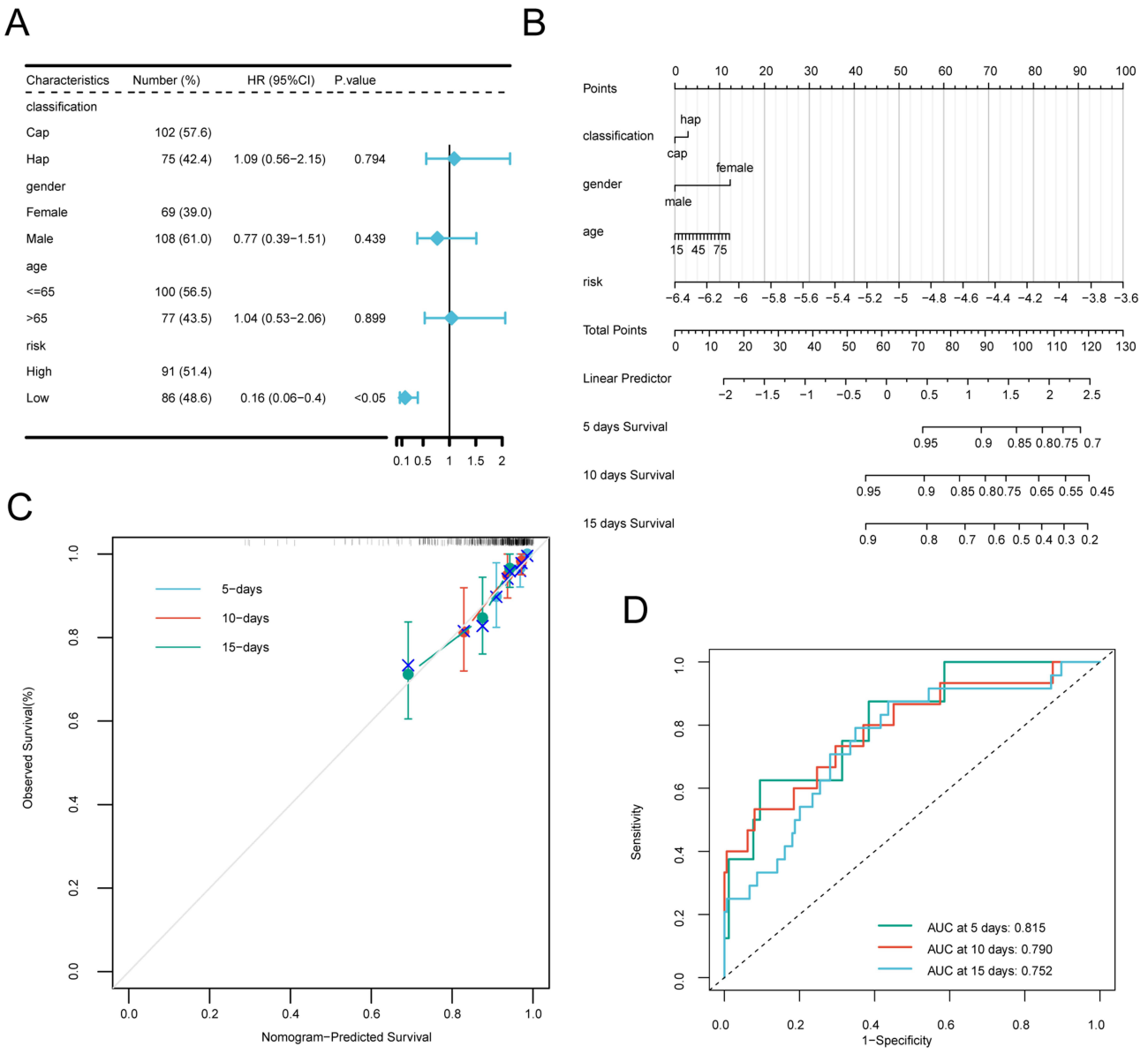

Figure 9 Risk score representing an independent predictor for clinical features. (**A**) Forest map displaying clinical features based on the univariate cox regression analysis. (**B**) Prediction model nomogram. The segment line displays the contribution of clinical factors to the outcome event, while the total score displays the cumulative scores derived from the individual scores of all variable values. The lower three lines illustrate the prognosis of the respective 5-, 10-, and 15-day survival periods at each value point. (**C**) The calibration curve of nomogram at 5-, 10-, and 15-days. (**D**) Receiver operating characteristic curves of the nomogram for the 5-, 10-, and 15-day survival periods. n=177, d=34, p=4, 50 subjects per group.

a pool of 54 vesicles and play a key role in cell-to-cell communication. Innate immune cell activation is a key factor governing the closely regulated process of leukocyte extracellular vesicle secretion.[30] Furthermore, our analysis of cellular communication networks indicated that the MHC-I signal was most enhanced in NK cells during sepsis-induced ARDS as opposed to sepsis alone. We also observed the hyperactivation of receptor-ligand networks between NK cells and $CD8^+$T cells, including MIF-(CD74+CXCR4) and HLA-B-CD8A. Our analysis showed that NK cells had the highest level of crosstalk with $CD8^+$T cells through the MIF and MHC-I pathways, indicating a proinflammatory role of $CD8^+$T cells in sepsis-induced ARDS development. MIF, a pivotal cytokine that binds to receptors such as CD74 in sepsis, impacts the host response to infection and may regulate inflammation processes.[31] MHC-I is a crucial complex that regulates the presentation of antigens to $CD8^+$T cells, thereby affecting $CD8^+$ T-cell responses.[29] These differences may be related to ARDS pathogenesis or the progression from sepsis to ARDS, offering a novel avenue of research for the treatment of sepsis-induced ARDS. Next,

https://doi.org/10.2147/JIR.S539379

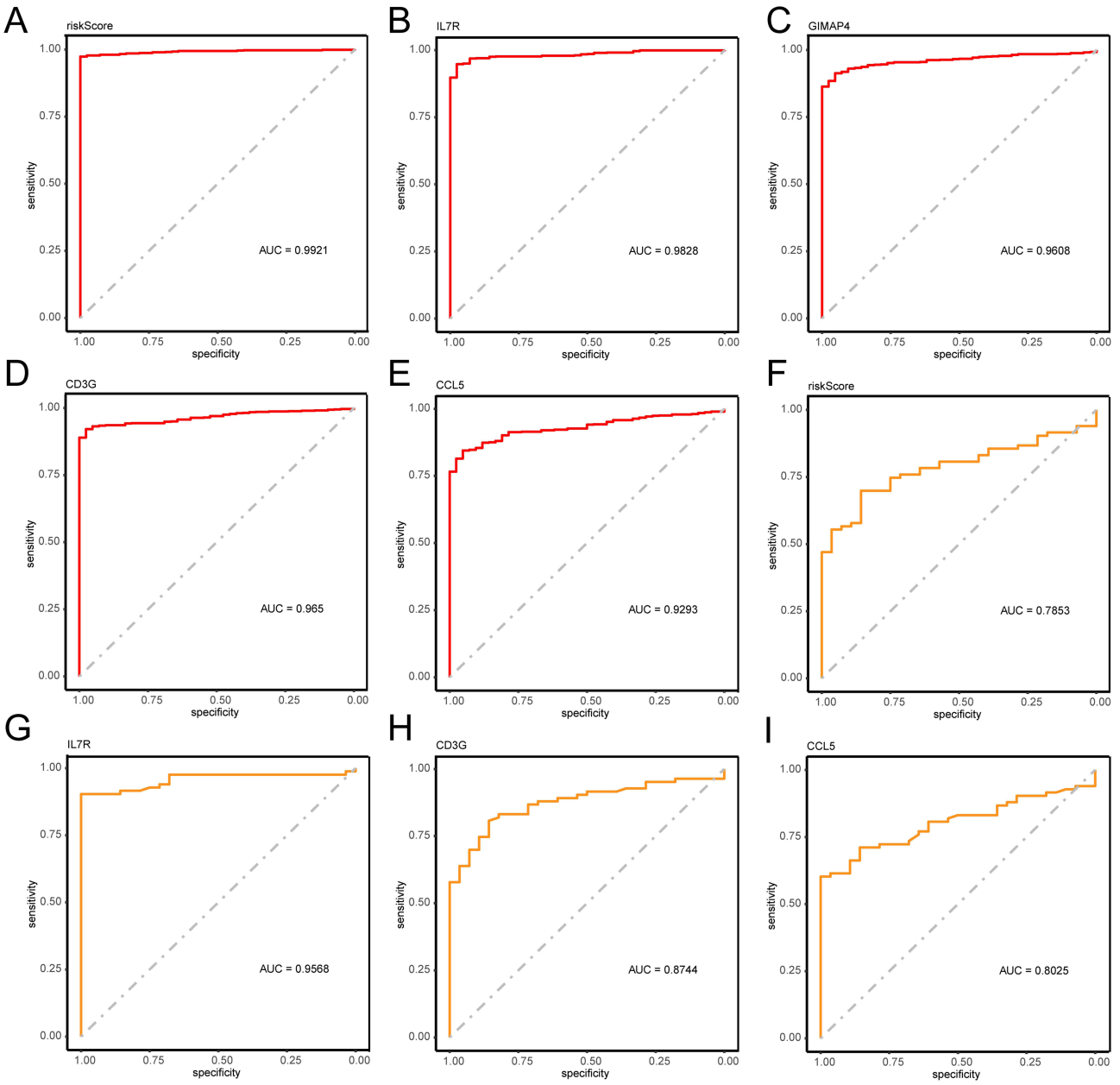

Figure 10 Diagnostic prediction of sepsis by riskScore and prognostic genes. (**A**) ROC curve of riskScore. (**B**) ROC curve of gene IL7R. (**C**) ROC curve of gene GIMAP4. (**D**) ROC curve of gene CD3G. (**E**) ROC curve of gene CCL5. (**F**) riskScore ROC curve in independent data set. (**G**) ROC curve of gene IL7R in an independent dataset. (**H**) ROC curve of gene CD3G in an independent dataset. (**I**) ROC curve of gene CCL5 in an independent dataset.

pyroptosis activity was assessed using the "AUCell" algorithm with the pyroptosis gene set obtained from various literature sources. Key genes regulating pyroptosis were identified. To elucidate potential PRG mechanisms, 38 hub genes were identified. Altogether, these findings highlight that PRGs are involved in important and complex immune microenvironments and processes in sepsis-induced ARDS and may be more responsive to immunotherapy.

Next, two groups were identified for the validation and broad application of the prognostic signature. Differentiation between low- and high-risk subpopulations is primarily attributed to a four-gene signature. Our results were consistently satisfactory in both cohorts. It successfully discriminated between patients in different risk subpopulations and identified those in the high-risk subgroup with poor prognosis. Statistically significant differences in the immune microenvironment were also found between those at low and high risk. Furthermore, the signature prognostic value for 5-, 10-, and 15- survival rates was satisfactory. Regarding our in-depth investigation into prognostic-signature-based immune-related disparities, our study

revealed significant upregulation of IL7R in CD4+ T cells and upregulation of CCL5 in CD8+ T, NK, and megakaryocyte progenitor cells. In terms of immune infiltration, the study showed that high-risk cases had a lower expression of activated CD8+ T, effector memory CD8+ T, and memory B cells than low-risk cases, whereas higher expression was observed in central memory CD8+ T cells. These data corroborate earlier study results.[32] The disease features CD4+, CD8+, and T helper 17 cell loss and regulatory T-cell upregulation. Liao et al[33] demonstrated a decrease in the number of activated B and CD8+ T cells in cases of sepsis. Within the surviving memory CD8+ T cell subpopulation, central memory CD8+ T cells excel at reestablishing the memory CD8+ T cell count and exhibit better proliferation during sepsis. The proliferation of central memory CD8+ T cells is linked to the numeric recuperation of pathogen-specific memory CD8+ T cells after lymphopenia caused by sepsis.[34] Therefore, we speculate that central memory CD8+ T cells play an essential role in sepsis-related ARDS. Hotchkiss et al[35] indicated that patients with sepsis show a severe deficiency of B-cells in sepsis. Within the category of mature B cells, memory B cells potentially serve as bridges connecting the innate and adaptive immune responses, with diminished counts observed in sepsis non-survivors.[36] Hence, for patients within the high-risk subpopulation, discrepancies in immune cell infiltration may correlate with a less favorable prognosis. The probability of survival was markedly reduced in patients classified in the high-risk category compared with their low-risk counterparts. Further studies are required to understand the complex interactions between genes and immune cells.

Pyroptosis is a genetically regulated form of cell death. Pyroptosis is triggered by distinct pathways when cells are exposed to various stimuli and is ultimately mediated by the GSDMD protein.[37] Subsequently, GO enrichment analyses revealed a significant association between immune-related BPs and PRGs. Several gene sets were identified as being significantly enriched within the sepsis group based on GSEA. In brief, the "JAK_STAT_SIGNALING_PATHWAY" is the set of genes that are regulated by JAK/STAT. This consists of a set of 156 genes, among which are associated IL-10 and IFN-γ and several other inflammatory cytokines. JAK/STAT is involved in many BPs including cell proliferation, differentiation, apoptosis and its regulation, immune response regulation, organ injury, and cardiac permeability in septic model.[38] The JAK-STAT signaling pathway mediated by type I interferons facilitates the transition from apoptosis to pyroptosis during influenza virus infection.[39]

Among the four genes associated with signatures (IL7R, GIMAP4, CD3G, and CCL5), IL7R expression is the defining characteristic of the "common lymphoid progenitor", but could also be found in macrophages.[40] IL7R participates in lymphoid development and function, and regulates T cell differentiation, development, and survival. IL7R transcription resumes after the CD4/CD8 double-positive stage, which is observed in peripheral T cells expressing CD4 or CD8.[41] Studies have demonstrated that IL7R levels are markedly reduced in sepsis, and introduced a diagnostic model for sepsis by identifying a gene signature that includes the IL7R hub genes.[42] Therefore, IL7R may be a promising marker for future studies. The chemokine gene CCL5, located on chromosome 17 and referred to as C-C motif chemokine ligand 5, is a potential therapeutic target for treating sepsis.[43] The hub gene, CCL5, a biomarker that may be useful for diagnosing and treating patients with sepsis, has been elucidated in previous studies.[44] CCL5 expression is notably increased in patients with sepsis compared to that in non-sepsis patients and is markedly associated with prognosis.[43,45] However, Frimpong et al revealed that children with sepsis exhibited significantly reduced levels of RANTES/CCL5 compared to children with malaria and febrile controls.[46] Additionally, CCR5 activation via the CCR5/PKA/CREB/NLRP1 pathway has been suggested to contribute to neuronal pyroptosis after mouse intracerebral hemorrhage. Therefore, it would be interesting to investigate the functions of CCL5 in the future. Another study discovered that the genes involved in T cells (CD3G and CCL5) were negatively linked to sequential organ failure and mortality in cases of sepsis.[47] CD3G directs the synthesis of the CD3 gamma polypeptide, a fundamental building block of the T-cell receptor-CD3 complex, combined with CD3 epsilon, delta, and zeta, along with T-cell receptor alpha/beta and gamma/delta heterodimers. This complex plays a fundamental role in linking antigen recognition to different cellular signaling pathways. In addition to its involvement in T-cell activation signal transduction, CD3G plays a crucial role in dynamically controlling TCR expression on the cell surface. CD3G was identified as a predictive biomarker for diagnosis in a robust model of neonatal early onset sepsis with bacterial infection.[48] GIMAP4 belongs to the GTPase family of immunity-associated proteins, and encodes a single protein. Schnell et al discovered that GIMAP4 induces programmed cell death, and that GIMAP4 phosphorylation is closely associated with apoptosis.[49] To the best of our knowledge, this is

the first study to identify GIMAP4 as a prognostic biomarker of pyroptosis in sepsis-related diseases. Therefore, it may play an important role in the development of sepsis-induced ARDS.

Correlation analysis was conducted on the relationship between pyroptosis and the septic immune environment. As indicated by our study, the expression of the majority of genes associated with the signature was correlated with immune cell infiltration levels. Importantly, correlation analysis illustrated a positive correlation between three of the four PRGs and activated $CD8^+$T cells. In addition, CD3G was positively correlated with effector memory $CD8^+$T cells, suggesting a close connection between pyroptosis and $CD8^+$T cells. However, the association between pyroptosis and septic $CD8^+$T-cells remains poorly understood. Studies have shown that $CD8^+$T cells can inhibit tumor growth by inducing ferroptosis and pyroptosis, prompting researchers to investigate the link between immune activation and tumor cell death mechanisms. Therefore, future studies should investigate $CD8^+$T cell pyroptosis in sepsis. Additional research is required to examine the potential impact of combination treatment on these immune cells. Analysis by Schnell et al showed that the expression levels of GIMAP4 in B, $CD4^+$T, $CD8^+$T, and natural killer cells were higher, but lower in macrophages and dendritic cells.[49] This is not in conflict with our study showing that GIMAP4 was negatively correlated with dendritic cells, macrophages, and natural killer cells. It is important to understand how the immune microenvironment interacts with various physiological processes during sepsis. Given that GIMAP4 is believed to be a regulator of the immune system, GIMAP4 may serve as a promising target for inflammatory suppression.

Recent studies have indicated that the classification of early-onset and late-onset neonatal sepsis varies across countries with different income levels.[50] This suggests that the aetiology and immune characteristics of sepsis are significantly dependent on the environment and population, which also emphasizes the need for further validation of the prognostic model we constructed in more multi-clinical center patient groups in the future. Another latest study employed systems biology approaches to uncover the common molecular mechanisms and key genes among sepsis, COVID-19, and ARDS in the elderly, and proposed potential therapeutic targets.[51] These findings share certain commonalities with the immune-related prognostic genes identified in our study, further supporting the core role of inflammation and immune regulation in sepsis-associated ARDS.

Therefore, our research results may provide important insights for future treatment strategies. Intervention measures targeting PRGs apoptosis may become a new direction for the treatment of septicemia-related ARDS, such as inhibiting specific PRGs or regulating related inflammatory pathways. In addition, considering the relationship between PRGs and immune regulation, formulating treatment strategies targeting immune function, such as optimizing the functions of T cells and B cells, may also help improve the prognosis of patients.

This study still has several limitations. First and foremost, the scope of our single-cell RNA sequencing analysis was constrained by a small sample size. While single-cell RNA sequencing analysis provides unparalleled resolution of cellular heterogeneity, the limited number of samples, may reduce the statistical power and generalizability of our findings. Second, the conclusions of this study are primarily derived from computational bioinformatics analyses of publicly available datasets. While we employed rigorous statistical methods and validated our prognostic model using an external dataset (GSE69528), this approach remains correlative. A significant limitation is the lack of experimental validation to establish causal relationships. The functional roles of the four identified signature genes in mediating pyroptosis and influencing the immune microenvironment in sepsis-induced ARDS have not been verified through in vitro or vivo experiments. Finally, while we performed multivariate analysis, our model may not have fully accounted for all sources of clinical heterogeneity (such as different infection sources, pre-existing comorbidities, etc). Future studies need to collect more multi-center, large-scale prospective clinical samples, combine in vitro and in vivo functional experiments, integrate multi-omics data, and in-depth explore the functional mechanistic role of key genes in the occurrence and development of the disease, so as to promote the application of research from computational prediction to clinical translation.

Conclusion

This study presents a groundbreaking gene signature that predicts the prognosis of patients with sepsis-induced ARDS, laying a substantial groundwork for future inquiries linking the immune response and PRGs in sepsis-induced ARDS.

Data Sharing Statement

The datasets presented in this study can be found in online repositories. The names of the repositories and links can be found in the article. The data that support the findings of this studyare available in the The Gene Expression Omnibus (GEO) (https://www.ncbi.nlm.nih.gov/geo/).

Funding

This work was supported by the Hubei Provincial Natural Science Foundation of China (No. 2022CFB565).

Disclosure

The authors declare that they have no known competing financial interests or personal relationships that could have appeared to influence the work reported in this paper.

References

1. Rudd KE, Johnson SC, Agesa KM, et al. Global, regional, and national sepsis incidence and mortality, 1990-2017: analysis for the global burden of disease study. *Lancet*. 2020;395(10219):200–211. doi:10.1016/S0140-6736(19)32989-7
2. Bellani G, Laffey JG, Pham T, et al. Epidemiology, patterns of care, and mortality for patients with acute respiratory distress syndrome in intensive care units in 50 countries. *JAMA*. 2016;315(8):788–800. doi:10.1001/jama.2016.0291
3. Sheu CC, Gong MN, Zhai R, et al. Clinical characteristics and outcomes of sepsis-related vs non-sepsis-related ARDS. *Chest*. 2010;138 (3):559–567. doi:10.1378/chest.09-2933
4. Xu XD, Chen JX, Zhu L, Xu ST, Jiang J, Ren K. The emerging role of pyroptosis-related inflammasome pathway in atherosclerosis. *Mol Med*. 2022;28(1):160. doi:10.1186/s10020-022-00594-2
5. Zhang MJ, Gao W, Liu S, et al. CD38 triggers inflammasome-mediated pyroptotic cell death in head and neck squamous cell carcinoma. *Am J Cancer Res*. 2020;10(9):2895–2908.
6. Masters SL, Gerlic M, Metcalf D, et al. NLRP1 inflammasome activation induces pyroptosis of hematopoietic progenitor cells. *Immunity*. 2012;37 (6):1009–1023. doi:10.1016/j.immuni.2012.08.027
7. Liu B, Wang Z, He R, et al. Buformin alleviates sepsis-induced acute lung injury via inhibiting NLRP3-mediated pyroptosis through an AMPK-dependent pathway. *Clin Sci*. 2022;136(4):273–289. doi:10.1042/CS20211156
8. Li G, Yan K, Zhang W, Pan H, Guo P. ARDS and aging: TYMS emerges as a promising biomarker and therapeutic target. *Front Immunol*. 2024;15:1365206. doi:10.3389/fimmu.2024.1365206
9. Stark R, Grzelak M, Hadfield J. RNA sequencing: the teenage years. *Nat Rev Genet*. 2019;20(11):631–656. doi:10.1038/s41576-019-0150-2
10. Butler A, Hoffman P, Smibert P, Papalexi E, Satija R. Integrating single-cell transcriptomic data across different conditions, technologies, and species. *Nat Biotechnol*. 2018;36(5):411–420. doi:10.1038/nbt.4096
11. Ye Y, Dai Q, Qi H. A novel defined pyroptosis-related gene signature for predicting the prognosis of ovarian cancer. *Cell Death Discov*. 2021;7 (1):71. doi:10.1038/s41420-021-00451-x
12. Latz E, Xiao TS, Stutz A. Activation and regulation of the inflammasomes. *Nat Rev Immunol*. 2013;13(6):397–411. doi:10.1038/nri3452
13. Karki R, Kanneganti TD. Diverging inflammasome signals in tumorigenesis and potential targeting. *Nat Rev Cancer*. 2019;19(4):197–214. doi:10.1038/s41568-019-0123-y
14. Ju A, Tang J, Chen S, Fu Y, Luo Y. Pyroptosis-related gene signatures can robustly diagnose skin cutaneous melanoma and predict the prognosis. *Front Oncol*. 2021;11:709077. doi:10.3389/fonc.2021.709077
15. Zheng J, Zhou Z, Qiu Y, et al. A pyroptosis-related gene prognostic index correlated with survival and immune microenvironment in glioma. *J Inflamm Res*. 2022;15:17–32. doi:10.2147/JIR.S341774
16. Qiu X, Mao Q, Tang Y, et al. Reversed graph embedding resolves complex single-cell trajectories. *Nat Method*. 2017;14(10):979–982. doi:10.1038/nmeth.4402
17. Karmaus PWF, Chen X, Lim SA, et al. Metabolic heterogeneity underlies reciprocal fates of T(H)17 cell stemness and plasticity. *Nature*. 2019;565 (7737):101–105. doi:10.1038/s41586-018-0806-7
18. Fang Z, Tian Y, Sui C, et al. Single-cell transcriptomics of proliferative phase endometrium: systems analysis of cell-cell communication network using cellchat. *Front Cell Develop Biol*. 2022;10:919731. doi:10.3389/fcell.2022.919731
19. Gene Ontology C. Gene ontology consortium: going forward. *Nucleic Acids Res*. 2015;43(Database issue):D1049–56. doi:10.1093/nar/gku1179
20. Friedman J, Hastie T, Tibshirani R. Regularization paths for generalized linear models via coordinate descent. *J Stat Softw*. 2010;33(1):1–22. doi:10.18637/jss.v033.i01
21. Subramanian A, Tamayo P, Mootha VK, et al. Gene set enrichment analysis: a knowledge-based approach for interpreting genome-wide expression profiles. *Proc Natl Acad Sci USA*. 2005;102(43):15545–15550. doi:10.1073/pnas.0506580102
22. Liberzon A, Birger C, Thorvaldsdóttir H, Ghandi M, Mesirov JP, Tamayo P. The Molecular Signatures Database (MSigDB) hallmark gene set collection. *Cell Systems*. 2015;1(6):417–425. doi:10.1016/j.cels.2015.12.004
23. Wu S, Lv X, Li Y, et al. Integrated machine learning and single-sample gene set enrichment analysis identifies a TGF-beta signaling pathway derived score in headneck squamous cell carcinoma. *J Oncol*. 2022;2022:3140263. doi:10.1155/2022/3140263
24. Ru B, Wong CN, Tong Y, et al. TISIDB: an integrated repository portal for tumor-immune system interactions. *Bioinformatics*. 2019;35 (20):4200–4202. doi:10.1093/bioinformatics/btz210
25. Ito K, Murphy D. Application of ggplot2 to pharmacometric graphics. *CPT*. 2013;2(10):e79.

26. Liang Q, Lin Q, Li Y, et al. Effect of SIS3 on extracellular matrix remodeling and repair in a lipopolysaccharide-induced ARDS rat model. *J Immunol Res*. 2020;2020:6644687. doi:10.1155/2020/6644687
27. Cheng Z, Abrams ST, Toh J, et al. The critical roles and mechanisms of immune cell death in sepsis. *Front Immunol*. 2020;11:1918. doi:10.3389/fimmu.2020.01918
28. Guo Y, Patil NK, Luan L, Bohannon JK, Sherwood ER. The biology of natural killer cells during sepsis. *Immunology*. 2018;153(2):190–202. doi:10.1111/imm.12854
29. Guo L, Shen S, Rowley JW, et al. Platelet MHC class I mediates CD8+ T-cell suppression during sepsis. *Blood*. 2021;138(5):401–416. doi:10.1182/blood.2020008958
30. Nyman TA, Lorey MB, Cypryk W, Matikainen S. Mass spectrometry-based proteomic exploration of the human immune system: focus on the inflammasome, global protein secretion, and T cells. *Expert Rev Proteom*. 2017;14(5):395–407. doi:10.1080/14789450.2017.1319768
31. Grieb G, Kim BS, Simons D, Bernhagen J, Pallua N. MIF and CD74 - suitability as clinical biomarkers. *Mini Rev Med Chem*. 2014;14(14):1125–1131. doi:10.2174/1389557515666150203143317
32. Chen Y, Qiu C, Cai W. Identification of key immune genes for sepsis-induced ARDS based on bioinformatics analysis. *Bioengineered*. 2022;13(1):697–708. doi:10.1080/21655979.2021.2012621
33. Liao W, Xiao H, He J, et al. Identification and verification of feature biomarkers associated with immune cells in neonatal sepsis. *Eur J Med Res*. 2023;28(1):105. doi:10.1186/s40001-023-01061-2
34. Jensen IJ, Li X, McGonagill PW, et al. Sepsis leads to lasting changes in phenotype and function of memory CD8 T cells. *eLife*. 2021;10:e70989.
35. Hotchkiss RS, Tinsley KW, Swanson PE, et al. Sepsis-induced apoptosis causes progressive profound depletion of B and CD4+ T lymphocytes in humans. *J Immunol*. 2001;166(11):6952–6963. doi:10.4049/jimmunol.166.11.6952
36. Duan S, Jiao Y, Wang J, et al. Impaired B-cell maturation contributes to reduced B cell numbers and poor prognosis in sepsis. *Shock*. 2020;54(1):70–77. doi:10.1097/SHK.0000000000001478
37. Man SM, Kanneganti TD. Gasdermin D: the long-awaited executioner of pyroptosis. *Cell Res*. 2015;25(11):1183–1184. doi:10.1038/cr.2015.124
38. Cai B, Cai JP, Luo YL, Chen C, Zhang S. The specific roles of JAK/STAT signaling pathway in sepsis. *Inflammation*. 2015;38(4):1599–1608. doi:10.1007/s10753-015-0135-z
39. Lee S, Hirohama M, Noguchi M, Nagata K, Kawaguchi A. Influenza A virus infection triggers pyroptosis and apoptosis of respiratory epithelial cells through the type I interferon signaling pathway in a mutually exclusive manner. *J Virol*. 2018;92(14). doi:10.1128/JVI.00396-18
40. Jacobsen FW, Veiby OP, Jacobsen SE. IL-7 stimulates CSF-induced proliferation of murine bone marrow macrophages and Mac-1+ myeloid progenitors in vitro. *J Immunol*. 1994;153(1):270–276. doi:10.4049/jimmunol.153.1.270
41. DeKoter RP, Schweitzer BL, Kamath MB, et al. Regulation of the interleukin-7 receptor alpha promoter by the Ets transcription factors PU.1 and GA-binding protein in developing B cells. *J Biol Chem*. 2007;282(19):14194–14204. doi:10.1074/jbc.M700377200
42. Liang G, Li J, Pu S, He Z. Screening of sepsis biomarkers based on bioinformatics data analysis. *J Healthc Eng*. 2022;2022:6788569. doi:10.1155/2022/6788569
43. Ness TL, Carpenter KJ, Ewing JL, Gerard CJ, Hogaboam CM, Kunkel SL. CCR1 and CC chemokine ligand 5 interactions exacerbate innate immune responses during sepsis. *J Immunol*. 2004;173(11):6938–6948. doi:10.4049/jimmunol.173.11.6938
44. Li M, Huang H, Ke C, et al. Identification of a novel four-gene diagnostic signature for patients with sepsis by integrating weighted gene co-expression network analysis and support vector machine algorithm. *Hereditas*. 2022;159(1):14. doi:10.1186/s41065-021-00215-8
45. Huang W, Huang L, Wen M, Fang M, Deng Y, Zeng H. Long non-coding RNA DILC is involved in sepsis by modulating the signaling pathway of the interleukin-6/signal transducer and activator of transcription 3/Toll-like receptor 4 axis. *Mol Med Rep*. 2018;18(6):5775–5783. doi:10.3892/mmr.2018.9559
46. Frimpong A, Owusu EDA, Amponsah JA, et al. Cytokines as potential biomarkers for differential diagnosis of sepsis and other non-septic disease conditions. *Front Cell Infect Microbiol*. 2022;12:901433. doi:10.3389/fcimb.2022.901433
47. Takahama M, Patil A, Richey G, et al. A pairwise cytokine code explains the organism-wide response to sepsis. *Nat Immunol*. 2024;25(2):226–239. doi:10.1038/s41590-023-01722-8
48. Bai Y, Zhao N, Zhang Z, Jia Y, Zhang G, Dong G. Identification and validation of a novel four-gene diagnostic model for neonatal early-onset sepsis with bacterial infection. *Eur J Pediatr*. 2023;182(3):977–985. doi:10.1007/s00431-022-04753-9
49. Heinonen MT, Kanduri K, Lähdesmäki HJ, Lahesmaa R, Henttinen TA. Tubulin-and actin-associating GIMAP4 is required for IFN-gamma secretion during Th cell differentiation. *Immunol Cell Biol*. 2015;93(2):158–166. doi:10.1038/icb.2014.86
50. Russell N, Barday M, Okomo U, Dramowski A, Sharland M, Bekker A. Early-versus late-onset sepsis in neonates-time to shift the paradigm? *Clin Microbiol Infect*. 2024;30(1):38–43. doi:10.1016/j.cmi.2023.07.023
51. Qian G, Fang H, Chen A, et al. A hub gene signature as a therapeutic target and biomarker for sepsis and geriatric sepsis-induced ARDS concomitant with COVID-19 infection. *Front Immunol*. 2023;14:257834.